Controllable vacuum Rabi splitting and optical bistability of multi-wave-mixing signal inside a ring cavity

Jiamin Yuan, Weikang Feng, Peiying Li, Xun Zhang, Yiqi Zhang, Huaibin Zheng, and Yanpeng Zhang*

Key Laboratory for Physical Electronics and Devices of the Ministry of Education and Shaanxi Key Lab of Information Photonic Technique, Xi'an Jiaotong University, Xi'an 710049, China

(Received 12 August 2012; published 17 December 2012)

We theoretically demonstrate the influence of dark and bright states on vacuum Rabi splitting (VRS) and optical bistability (OB) of the multi-wave-mixing (MWM) process in a collective four-level atomic-cavity coupling system. We numerically investigate the multidressed VRS and OB behavior of the zero- and high-order transmitted cavity modes of MWM signals. A further study demonstrates that VRS and self-Kerr nonlinearity OB can coexist and compete with each other in a cascade relationship, based on which we achieve the goal to control VRS and OB simultaneously through the dark state in the atomic system.

DOI: 10.1103/PhysRevA.86.063820 PACS number(s): 42.50.Gy, 32.80.Qk, 42.65.−k

I. INTRODUCTION

Electromagnetically induced transparency (EIT) [1–3] can effectively decrease the absorption of incident beams and has been researched since it may have potential applications in slow light [4], photon generation, transmission and information storage [5,6], quantum communication [7], and nonlinear optics and wave-mixing processes [8]. Dark state and EIT can be used in quantum interference and result in form-stable coupled excitations of light and matter associated with the propagation of quantum fields under EIT, which have been termed *dark-state polaritons* [9].

Moreover, vacuum Rabi splitting (VRS) [10] has been reported in a strongly coupled single two-level atom-cavity system [11], where the frequency distance of the VRS is given by $2g$ with single-atom coupling strength g. When N two-level atoms collectively interact with the cavity mode [12], the coupling strength can be increased as $G = g\sqrt{N}$ and the distance of VRS for the collectively coupled atom-cavity system will be $2G$ [13].

Recently, studies on atom-cavity interactions have been extended to a more composite system with an optical cavity and coherently prepared multilevel atoms [14], in which a narrow central peak was observed beside two broad sidebands (representing VRS) and can be well explained by the intracavity dispersion properties [15]. When the atom-cavity interaction reaches the "superstrong-coupling" condition with atom-cavity coupling strength G to be near or larger than the cavity free spectral range, multi-normal-mode splitting can be observed and well explained by the linear-dispersion enhancement due to the largely increased atomic density in the cavity [16,17].

Inspired by the intracavity phenomenon that quantum bright correlated light beams can be produced by driving an optical parametric oscillator (OPO) above its threshold [18,19], the bright correlated beams with off-resonance four-wave mixing (FWM) process have also been experimentally demonstrated [20]. In addition, experimental studies of coherently prepared atoms confined in a cavity have led the observations of the EIT line width narrowing [21] and coherent control of optical bistability (OB) and multistability [22].

On the other hand, the dressed MWM process in the corresponding EIT window has attracted a lot of attention in the past several years [23,24]. Recently, we have observed Autler-Townes (AT) splitting of the four-wave mixing (FWM) signals with dressing effects [25,26] generated in a multilevel atomic system. We have also observed the evolution of the enhancement (bright state) and suppression (dark state) in FWM processes by controlling the frequency detuning of the additional laser field [27,28]. Considering the origin of VRS and OB, and the application of the dark state in the MWM process, we deduce that dark and bright states can affect the properties of VRS and OB behavior in our proposed atom-cavity system and make that the focus of our research.

In this paper, we first investigate the relationship of VRS and OB of cavity MWM signals and achieve the goal to control VRS and OB simultaneously through the coherent control of dark and bright states, and get the inclined VRS. Studies on the multidressed VRS and OB behavior of the zero- and high-order transmitted cavity MWM signal in the coupled system consisting of a specific ring cavity and reverse Y-type four-level atoms assembly are presented, with VRS coming from the atom-cavity collective effect induced by high atom density, while OB behavior comes from the self-Kerr nonlinearity effect (feedback effect); the influences of dark and bright states are involved in detail. In addition, we show the linear gains and thresholds for the generated bright correlated light beams in lambda (Λ) and cascade (Ξ) subsystems in an OPO process and further discuss the OB thresholds in our optical parametric amplification (OPA) MWM process, which can bring about interesting applications in quantum information processing.

This paper is organized as follows. In Sec. II, we describe the basic theory for this work. In Sec. III, we first show the multidressed VRS of the transmitted cavity MWM signal in the linearity situation and the corresponding avoided-crossing plots with suppression and enhancement of the generated MWM signal in cavity. In Sec. IV, we present the high-order mode splitting and avoided-crossing plots of the transmitted cavity MWM signal with or without another dressing effect. These phenomena result from the atom-cavity collective effect and superstrong-coupling strength. In Sec. V, we show the linear gains and thresholds for the generated bright correlated light beams in the OPO process. In Sec. VI, we show the OB

*ypzhang@mail.xjtu.edu.cn

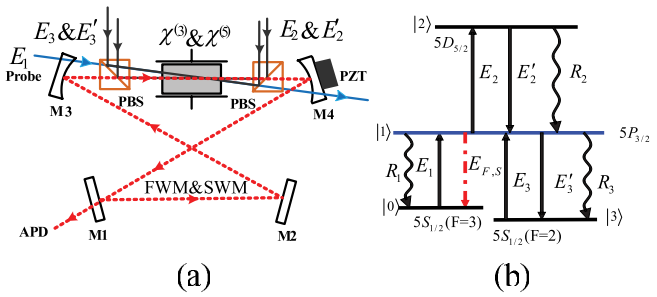

FIG. 1. (Color online) (a) A schematic diagram of a ring cavity containing the four-level atoms coupled with coherent external probe and control fields. The optical cavity length, which is fixed on atomic transition frequency, can be adjusted by a PZT mounted on the mirror M4. The frequency of the input laser (as probe light) is scanned to measure the transmission spectra. (b) Scheme of four-level atomic system.

behavior of the zero- and high-order transmitted cavity MWM signal resulting from the self-Kerr nonlinearity effect of the MWM field. Finally, in Sec. VII, we give the conclusion.

II. BASIC THEORY

We theoretically study a cavity-atom coupling system consisting of rubidium atoms confined in the four-mirror-formed mode volume with a length of $L_c = 17$ cm [Fig. 1(a)]. The mirrors M3 and M1 are input and output mirrors with a radius of 50 mm, whose reflectance r_3 (r_1) and transmittance t_3 (t_1) fulfill the condition $r_i^2 + t_i^2 = 1$ ($i = 1,3$), while the mirrors M2 and M4 are high-quality reflectors. Cavity frequency scanning and locking can be implemented by a piezoelectric transducer (PZT) behind M4. The length of the rubidium vapor cell including the Brewster windows is $L_a = 7$ cm. The cell is wrapped in μ-metal sheets to shield from external magnetic fields and a heat tape is placed outside the sheets for controlling the temperature to influence the atomic density. Since we do not consider Doppler effects in this paper, our analysis is also suitable for the ring or standing-wave cavity.

A reverse-Y energy level system as shown in Fig. 1(b) is constructed with four energy levels [$|0\rangle 5S_{1/2}(F = 3)$, $|1\rangle 5P_{3/2}$, $|2\rangle 5D_{5/2}$, $|3\rangle 5S_{1/2}(F = 2)$]. In this atomic system, a horizontally polarized weak probe field E_1 (frequency ω_1, wave vector $\mathbf{k}_1$, and Rabi frequency G_1) probes the lower transition $|0\rangle \rightarrow |1\rangle$. Two vertically polarized coupling fields E_2 (ω_2, $\mathbf{k}_2$, and G_2) and E_2' (ω_2, $\mathbf{k}'_2$, and G_2') propagate in the opposite direction of E_1, and drive the upper transition $|1\rangle \rightarrow |2\rangle$. Two additional vertically polarized coupling fields E_3 (ω_3, $\mathbf{k}_3$, and G_3) and E_3' (ω_3, $\mathbf{k}'_3$, and G_3') propagate in the same direction as E_1, and drive the transition $|3\rangle \rightarrow |1\rangle$. There will be two EIT windows in ladder-type subsystems $|0\rangle \rightarrow |1\rangle \rightarrow |2\rangle$ and $|0\rangle \rightarrow |1\rangle \rightarrow |3\rangle$, both satisfying the two-photon Doppler-free condition. Moreover, there will be two four-wave mixing (FWM) processes, E_{F2} (satisfying $\mathbf{k}_{F2} = \mathbf{k}_1 + \mathbf{k}_2 - \mathbf{k}'_2$) and E_{F3} ($\mathbf{k}_{F3} = \mathbf{k}_1 + \mathbf{k}'_3 - \mathbf{k}_3$); and four six-wave mixing (SWM) processes, E_{S2} ($\mathbf{k}_{S2} = \mathbf{k}_1 + \mathbf{k}' + \mathbf{k}'_3 - \mathbf{k}_3 + \mathbf{k}_2 - \mathbf{k}_2$), E'_{S2} ($\mathbf{k}'_{S2} = \mathbf{k}_1 + \mathbf{k}'_3 - \mathbf{k}_3 + \mathbf{k}'_2 - \mathbf{k}'_2$), E_{S3} ($\mathbf{k}_{S3} = \mathbf{k}_1 + \mathbf{k}_2 - \mathbf{k}'_2 + \mathbf{k}_3 - \mathbf{k}_3$), and E'_{S3} ($\mathbf{k}'_{S3} = \mathbf{k}_1 + \mathbf{k}_2 - \mathbf{k}'_2 + \mathbf{k}'_3 - \mathbf{k}'_3$), generating in this system, which are all horizontally polarized. Such MWM signals propagate in the same direction as E_3', and can circulate in the ring cavity according to the cavity configuration. In our model the total electromagnetic field can be written as $E = E_p e^{i\omega_1 t} + E_2 e^{i\omega_2 t} + E_2^* e^{i\omega_2 t} + E_3 e^{i\omega_3 t} + E_F e^{i\omega_1 t} + E_S e^{i\omega_1 t} + \text{c.c.}$ Generally, the density matrix elements related with FWM (SWM) signals can be obtained by solving the density-matrix equations. Especially, when E_3 (E_3') are blocked, via the simple perturbation chain $\rho_{00}^{(0)} \xrightarrow{\omega_1} \rho_{10}^{(1)} \xrightarrow{\omega_2} \rho_{20}^{(2)} \xrightarrow{-\omega_2} \rho_{10}^{(3)}$, we can obtain the simple third-order density element $\rho_{F2}^{(3)} = G_{F2}/[d_2 d_1^2]$ for E_{F2} (its intensity $I_{F2} \propto |\rho_{F2}^{(3)}|^2$), where $G_{F2} = -iG_1G_2(G_2')^* \exp(i\mathbf{k}_{F2} \cdot \mathbf{r})$, $d_1 = \Gamma_{10} + i\Delta_1$, and $d_2 = \Gamma_{20} + i(\Delta_1 + \Delta_2)$; $\Delta_i = \Omega_i - \omega_i$ is frequency detuning with resonance frequency Ω_i and Γ_{ij} is the transverse relaxation rate between states $|i\rangle$ and $|j\rangle$. If E_2 (or E_2') is strong enough, via the singly dressed perturbation chain $\rho_{00}^{(0)} \xrightarrow{\omega_1} \rho_{G_2\pm 0}^{(1)} \xrightarrow{\omega_2} \rho_{20}^{(2)} \xrightarrow{-\omega_2} \rho_{G_2\pm 0}^{(3)}$, we can obtain the singly dressed third-order density element $\rho_{SDF2}^{(3)} = G_{F2}/[d_2(d_1 + |G_2|^2/d_2)^2]$ for E_{F2} (the intensity $I_{F2} \propto |\rho_{SDF2}^{(3)}|^2$). In the dressed FWM processes E_{F2}, E_2 (or E_2') not only generates but also dresses the signal E_{F2}, so we refer to this dressing effect as the *internal dressing*. Then with E_3 turned on, the simple SWM process can be described by the perturbation chain $\rho_{00}^{(0)} \xrightarrow{\omega_1} \rho_{10}^{(1)} \xrightarrow{-\omega_3} \rho_{30}^{(2)} \xrightarrow{\omega_3} \rho_{10}^{(3)} \xrightarrow{\omega_2} \rho_{20}^{(4)} \xrightarrow{-\omega_2} \rho_{10}^{(5)}$, and the corresponding density element is $\rho_{S3}^{(5)} = G_{S3}/[d_2 d_3 d_1^3]$ for E_{S3} (its intensity $I_{S3} \propto |\rho_{S3}^{(5)}|^2$), where $G_{S3} = iG_1G_2(G_2')^*G_3G_3^* \exp(i\mathbf{k}_{S3} \cdot \mathbf{r})$ and $d_3 = \Gamma_{30} + i(\Delta_1 - \Delta_3)$. If E_2 (or E_2') and E_3 are all strong enough, the doubly dressed E_{F2} [internal- and external-dressing effects of E_2 (or E_2') and E_3, respectively] and E_{S3} [internal-dressing effect of both E_2 (or E_2') and E_3] can be generated simultaneously. Via the perturbation chains $\rho_{00}^{(0)} \xrightarrow{\omega_1} \rho_{(G_2\pm G_3\pm)0}^{(1)} \xrightarrow{\omega_2} \rho_{20}^{(2)} \xrightarrow{-\omega_2} \rho_{(G_2\pm G_3\pm)0}^{(3)}$ and $\rho_{00}^{(0)} \xrightarrow{\omega_1} \rho_{(G_2\pm G_3\pm)0}^{(1)} \xrightarrow{-\omega_3} \rho_{30}^{(2)} \xrightarrow{\omega_3} \rho_{(G_2\pm G_3\pm)0}^{(3)} \xrightarrow{\omega_2} \rho_{20}^{(4)} \xrightarrow{-\omega_2} \rho_{(G_2\pm G_3\pm)0}^{(5)}$, we can obtain the doubly dressed density elements $\rho_{DDF2}^{(3)} = G_{F2}/[d_2(d_1 + |G_2|^2/d_2 + |G_3|^2/d_3)^2]$ for E_{F2} (its intensity $I_{F2} \propto |\rho_{DDF2}^{(3)}|^2$) and $\rho_{DDS3}^{(5)} = G_{S3}/[d_2 d_3 (d_1 + |G_2|^2/d_2 + |G_3|^2/d_3)^3]$ for E_{S3} (the intensity $I_{S3} \propto |\rho_{DDS3}^{(5)}|^2$). The two doubly dressed MWM signals can be distinguished in different EIT windows. Next, we set the rubidium atomic gas cell in the ring cavity [Fig. 1(a)], in which the cavity polariton is formed in the interaction between the cavity mode and the N identical atoms with four energy levels. The identical atom assemblies are most easily described as a homogeneously broadened medium in the small-gain limit. Set a as the cavity field, coupled with the transition $|0\rangle \rightarrow |1\rangle$, to form the cavity mode with the generated FWM (SWM) signal according to the cavity configuration. Under the weak-cavity field limitation and with all the atoms initially in the ground state $|0\rangle$, if the system is in equilibrium state, the transmitted cavity mode induced by FWM (SWM) and doubly dressed by E_2 (or E_2') and E_3 can be obtained as

$$a_{FWM} = \frac{-g\sqrt{N}G_{F(S)}}{d_4\left(d_1 + \frac{g^2N}{d_4} + \frac{|G_2|^2}{d_2} + \frac{|G_3|^2}{d_3}\right)}, \tag{1}$$

where $d_4 = i(\Delta_1 - \Delta_{ac}) + \gamma$.

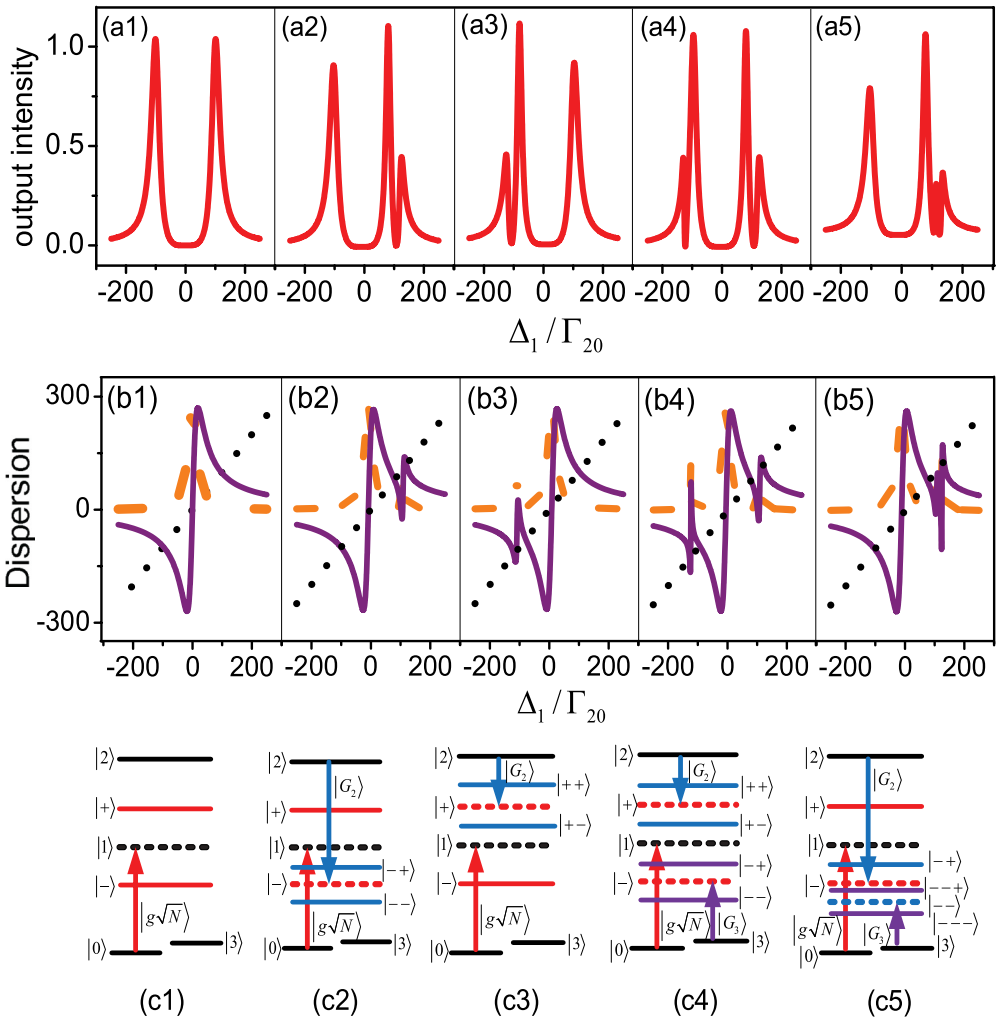

FIG. 2. (Color online) (a) Theoretically calculated transmitted cavity FWM (SWM) spectra versus Δ_1 for $\Delta_{ac} = 0$. (a1) Normal VRS when the powers of coupling fields E_2 and E_2' are relatively weak and E_3 and E_3' are blocked; (a2) and (a3) the AT splitting based on normal VRS when the power of E_2 (or E_2') is strong enough and E_3 and E_3' are blocked for (a2) $\Delta_2/\Gamma_{20} = -100$ and (a3) $\Delta_2/\Gamma_{20} = 100$, respectively; (a4) and (a5) the AT splitting effect of the transmitted cavity FWM (SWM) when the powers of E_2 (or E_2') and E_3 are sufficiently strong and E_3' is blocked for (a4) $\Delta_2/\Gamma_{20} = -100$, $\Delta_3/\Gamma_{20} = -100$, and (a5) $\Delta_2/\Gamma_{20} = -100$, $\Delta_3/\Gamma_{20} = 120$, respectively. (b) Theoretical plots of intracavity dispersion curves (solid curves); absorption (dashed curves); and detuning lines (dotted lines) versus Δ_1 corresponding to (a). (c) Dressed-state energy level diagrams corresponding to (a).

III. VRS OF ZERO-ORDER MODE

In this section, we discuss multidressed VRS of zero-order cavity mode (single-mode) of the MWM process in the coupled atom-cavity system based on the master equation formalism theory. This phenomenon is derived from the atom-cavity coupling effect, reflected mainly by g^2N in the denominator in Eq. (1), which shows a self-dressing effect for both coming from the atom-cavity coupling effect and dressing the cavity field in return. Meanwhile, we also analyze the related suppression (dark state) and enhancement (bright state) phenomena by scanning the frequency detuning of one dressing field.

A. Multidressed VRS

In this part, we show the normal VRS and the AT splitting based on VRS of the transmitted cavity MWM signal by scanning the probe detuning. Figure 2 is the transmitted cavity spectra versus the probe frequency detuning while the cavity field is tuned to resonate with the atomic transition $|0\rangle \rightarrow |1\rangle$ ($\Delta_{ac} = 0$). First, when E_2 and E_2' are turned on but the their powers are relatively weak [i.e., not considering the dressing effect of $E_2(E_2')$] as shown in Fig. 2(a1), the transmitted cavity FWM spectrum exhibits two peaks (representing two cavity-atom polaritons), forming normal VRS of atom-cavity system with separation $2g\sqrt{N}$ in frequency due to the self-dressing effect of g^2N (atom-cavity coupling effect). The two eigenvalues corresponding to dressed states $|\pm\rangle$ induced by g^2N are $\lambda_\pm = \pm g\sqrt{N}$ (due to $\Delta_{ac} = 0$, measured from $|1\rangle$) after diagonalizing the interaction Hamiltonian. The two peaks of the transmitted cavity FWM signal [Fig. 2(a1)] correspond, from left to right, to the dressed states $|+\rangle$ and $|-\rangle$, respectively [Fig. 2(c1)]. Next, when the power of E_2 becomes so strong that its dressing effect must be taken into account

and its frequency matches the polariton resonance [$\Delta_2 = -g\sqrt{N} = -100\Gamma_{20}$ and $\Delta_2 = g\sqrt{N} = 100\Gamma_{20}$ in Figs. 2(a2) and 2(a3), respectively], the AT splitting effect based on the VRS is induced. Due to the dressing effects of g^2N and E_2, the two-peak spectrum in Fig. 2(a1) turns into a three-peak spectrum in Figs. 2(a2) and 2(a3). When E_2 resonates with the dressed state $|-\rangle$ with $\Delta_2 = -g\sqrt{N} = -100\Gamma_{20}$, a pair of new dressed states $|-\pm\rangle$ appears as shown in Fig. 2(c2), and the corresponding eigenvalues are $\lambda_{-\pm} = \pm G_2$ (measured from $|-\rangle$) with separation $2G_2$. When E_2 couples with the dressed state $|+\rangle$ with $\Delta_2 = g\sqrt{N} = 100\Gamma_{20}$, the dressed states $|+\pm\rangle$ appear as shown in Fig. 2(c3), and the corresponding eigenvalues are $\lambda_{+\pm} = \pm G_2$ (measured from $|+\rangle$) with separation $2G_2$. The three peaks of the transmitted cavity FWM signal in Figs. 2(a2) and 2(a3) correspond, from left to right, to the dressed states $|+\rangle, |-+\rangle, |--\rangle$ [Fig. 2(c2)] and $|++\rangle, |+-\rangle, |-\rangle$ [Fig. 2(c3)], respectively. Finally, with the field E_3 turned on and set as a strong field, the dressing effect of E_3 must be considered. As a result, the triply dressed transmitted cavity FWM (SWM) signal with four peaks is obtained, as shown in Figs. 2(a4) and 2(a5). The four peaks in Fig. 2(a4), from left to right, correspond to the dressed states $|++\rangle$, $|+-\rangle$, $|-+\rangle$ and $|--\rangle$, where the dressed state $|+\rangle$ induced by g^2N is split into $|++\rangle$, $|+-\rangle$ by E_3 ($\Delta_3 = -g\sqrt{N} = -100\Gamma_{20}$) with eigenvalues $\lambda_{+\pm} = \pm G_3$ (measured from $|+\rangle$), while $|-\rangle$ is split into $|-+\rangle$, $|--\rangle$ by E_2 ($\Delta_2 = -g\sqrt{N} = -100\Gamma_{20}$) with eigenvalues $\lambda_{-\pm} = \pm G_2$ (measured from $|-\rangle$), respectively, as shown as Fig. 2(c4). However, the four peaks in Fig. 2(a5), from left to right, correspond to the dressed states $|+\rangle$, $|-+\rangle$, $|--+\rangle$, and $|---\rangle$, where $|-\rangle$ is split into $|-+\rangle$, $|--\rangle$ by E_2 ($\Delta_2 = -g\sqrt{N} = -100\Gamma_{20}$) with $\lambda_{-\pm} = \pm G_2$ (measured from $|-\rangle$), and further $|--\rangle$ is split into $|--+\rangle$ and $|---\rangle$ by E_3 ($\Delta_3 = g\sqrt{N} + G_2 = 120\Gamma_{20}$) with $\lambda_{--\pm} = \pm G_3$ (measured from $|--\rangle$), as shown in Fig. 2(c5). Here, we only give the resonant case, in which the dressing field resonates with either naked energy level or the dressed energy level dressed by another dressing field, and other cases without resonant splitting can also be obtained by adjusting the frequency detuning of the dressing fields.

Moreover, since the transmitted cavity FWM (SWM) signal can be determined by the corresponding absorption and dispersion characteristics [15], now we analyze the cavity transmission signals via the intracavity dispersion curves (solid), absorption curves (dashed), and detuning lines (dotted) shown in Figs. 2(b1)–2(b5), corresponding to Figs. 2(a1)–2(a5). Generally, the intersecting points of the detuning line and dispersion curve represent corresponding peaks in transmission spectra. In Fig. 2(b1), there are three intersecting points, while in the transmitted cavity spectrum in Fig. 2(a1), there are only two peaks corresponding to the bilateral intersections in Fig. 2(b1). The disappearance of the peak corresponding to the middle intersecting point results from the larger absorption [dashed curve in Fig. 2(b1)] at $\Delta_1/\Gamma_{20} = 0$. For the other cases shown as Figs. 2(b2)–2(b5), corresponding to Figs. 2(a2)–2(a5), the explanations are the same as that for Fig. 2(b1). The analysis above indicates that the explanation from the dressing energy diagram in Fig. 2(c) is in accordance with that from the intracavity dispersion and absorption properties in Fig. 2(b).

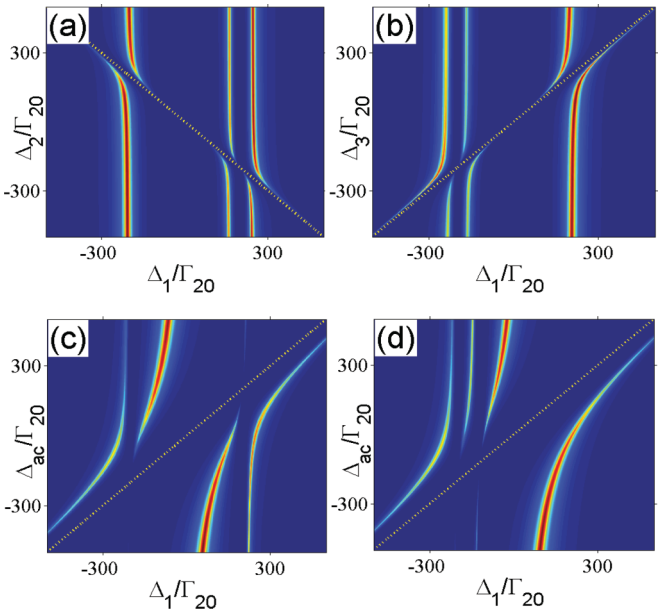

FIG. 3. (Color online) The transmitted cavity FWM (SWM) signal as a function of Δ_1 and different frequency detunings of dressing field for Δ_2 (a), Δ_3 (b), and Δ_{ac} [(c) and (d)], respectively, when E_3' is blocked. The parameters used in the theoretical plots are (a) $\Delta_3/\Gamma_{20} = 200$, (b) $\Delta_2/\Gamma_{20} = 200$, (c) $\Delta_2/\Gamma_{20} = \Delta_3/\Gamma_{20} = 200$, and (d) $\Delta_2/\Gamma_{20} = 200$, $\Delta_3/\Gamma_{20} = -120$.

B. Avoided-crossing plots

In order to investigate the transmitted cavity signals influenced by the probe field and the other coupling field simultaneously, we present the avoided-crossing plots in detail. Figure 3 shows the transmitted cavity FWM (SWM) signal as a simultaneous function of Δ_1 and different frequency detunings of dressing fields. The typical avoided-crossing shape in each plot clearly expresses the dark and bright states in the transmitted process in the atom-cavity system. For instance, when scanning Δ_1 and Δ_2 with other detunings fixed, as illustrated in Fig. 3(a), the cavity field induces the primary splitting (VRS); E_3 induces the secondary splitting (AT splitting, corresponding to $\Delta_1/\Gamma_{20} = 200$), and E_2 induces the triple splitting with minimal distance at $\Delta_2 = -\Delta_1 = g\sqrt{N}$, $-g\sqrt{N} + G_3$, and $-g\sqrt{N} - G_3$ from left to right, by scanning Δ_1 (horizontal axis). Simultaneously, by scanning Δ_2 (vertical axis), the transmitted cavity FWM (SWM) signal is suppressed (dark state) along the dotted dividing line $\Delta_1 + \Delta_2 = 0$, which exactly satisfies the suppression condition resulting from the dressing effect of E_2 in this process. Similarly, by scanning Δ_1 and Δ_3 [Fig. 3(b)], and Δ_1 and Δ_{ac} [Figs. 3(c) and 3(d) with different Δ_2 and Δ_3], the transmitted cavity FWM (SWM) signals are suppressed significantly at $\Delta_1 - \Delta_3 = 0$ (suppression condition from the dressing effect of E_3) and $\Delta_1 - \Delta_{ac} = 0$ (from the self-dressing effect of g^2N) along the dividing lines in Figs. 3(b)–3(d), respectively.

C. Suppression and enhancement of MWM

We next study the suppression (dark state) and enhancement (bright state) effect of the transmitted cavity signal of doubly dressed FWM and triply dressed FWM (SWM) in an

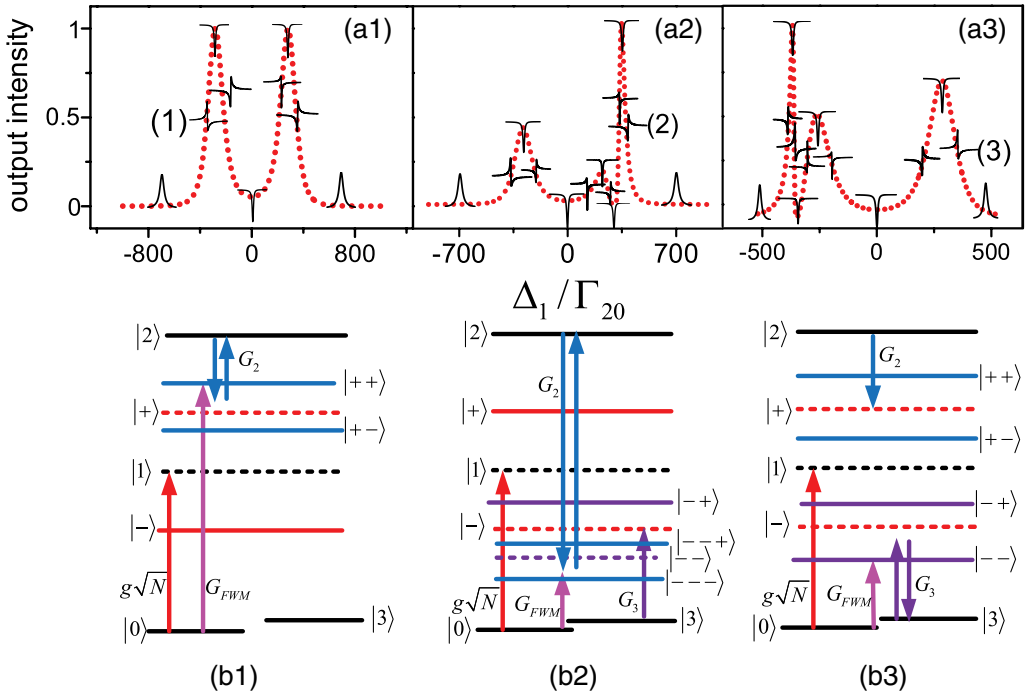

FIG. 4. (Color online) (a) The transmitted cavity spectra of the generated FWM (or SWM) dressed by fields a and $E_2\,(E_2')$ (a1), and fields a, $E_2\,(E_2')$, and E_3 [(a2) and (a3)] versus Δ_2 [(a1) and (a2)] and Δ_3 (a3) with different Δ_1. The dashed profiles are cavity transmission signals versus Δ_1. (b1)–(b3) The dressed energy level diagrams of the cavity transmission signal corresponding to (a1)–(a3).

atom-cavity system by scanning Δ_2 or Δ_3 at different Δ_1/Γ_{20}, illustrated in Figs. 4(a1)–4(a3). The baselines represent the transmitted cavity signal undressed by the scanning field. We call the dips lower than the baselines as suppression and peaks higher than the baselines as enhancement.

Figure 4(a1) shows the suppression and enhancement of the transmitted cavity signal dressed by g^2N and $E_2(E_2')$ when Δ_2 is scanned at different Δ_1 within an atom-cavity subsystem $|0\rangle - |1\rangle - |2\rangle$ (FWM signal E_{F2}) with E_3 and E_3' blocked. The dashed double-peak global profile in Fig. 4(a1), induced by g^2N, is the cavity transmitted FWM signal without the dressing effect of $E_2(E_2')$. If Δ_1 is set from negative to positive, the cavity transmitted FWM signal shows the evolution from all enhancement ($\Delta_1/\Gamma_{20} = -700$), to left enhancement and right suppression ($\Delta_1/\Gamma_{20} = -331$), to all suppression ($\Delta_1/\Gamma_{20} = -257$), to left suppression and right enhancement ($\Delta_1/\Gamma_{20} = -200$), to all suppression ($\Delta_1/\Gamma_{20} = 0$), to left enhancement and right suppression ($\Delta_1/\Gamma_{20} = 198$), to all suppression ($\Delta_1/\Gamma_{20} = 257$), to left suppression and right enhancement ($\Delta_1/\Gamma_{20} = 325$), to all enhancement ($\Delta_1/\Gamma_{20} = 700$), as shown in Fig. 4(a1). Such evolution is caused by the interaction between the dressing fields g^2N and $E_2\,(E_2')$. Here we only take curve (1) in Fig. 4(a1) to analyze in detail. Under the self-dressing effect of g^2N, $|1\rangle$ will be split into two dressed states $|\pm\rangle$, and $|+\rangle$ will be split into two secondary-dressed states $|+\pm\rangle$ in the region $\Delta_1 < 0$ by $E_2\,(E_2')$. For the curve (1) ($\Delta_1/\Gamma_{20} = -331$), the transmitted cavity signal can resonate with $|++\rangle$ when Δ_2 is scanned if the enhancement condition $\Delta_1 + \lambda_+ + \lambda_{++} = 0$ is satisfied, where $\lambda_+ = g\sqrt{N}$ and $\lambda_{++} = (\Delta_2 - \lambda_+)/2 + \sqrt{(\Delta_2 - \lambda_+)^2/4 + |G_2|^2}$, and then two-photon resonance of the transmitted cavity signal occurs if the suppression condition $\Delta_1 + \Delta_2 = 0$ is satisfied. As a result, the transmitted cavity signal shows left enhancement and right suppression, as illustrated by curve (1) and Fig. 4(b1). Other curves in Fig. 4(a1) showing different suppression and enhancement can be explained similarly to curve (1), so we only give their suppression (due to two-photon resonance) and enhancement (due to the resonance with dressed states) conditions as $\Delta_1 + \Delta_2 = 0$ and $\Delta_1 + \lambda_+ + \lambda_{++} = 0$ for $\Delta_1 < 0$, and $\Delta_1 + \Delta_2 = 0$ or $\Delta_1 + \lambda_- + \lambda_{-\pm} = 0$ for $\Delta_1 > 0$, where $\lambda_\pm = \pm g\sqrt{N}$ and $\lambda_{\pm\pm} = (\Delta_2 - \lambda_\pm)/2 \pm \sqrt{(\Delta_2 - \lambda_\pm)^2/4 + |G_2|^2}$. The results of Fig. 4(a1) in $\Delta_1 < 0$ and $\Delta_1 > 0$ regions have symmetric centers $\Delta_1/\Gamma_{20} = \mp 257$, respectively, where the transmitted cavity signals are all purely suppressed.

Next we study the transmitted cavity signal triply dressed by g^2N, $E_2(E_2')$, and E_3 when Δ_2 is scanned at different Δ_1 within an atom-cavity system [Fig. 1(b)] with E_3' blocked as shown in Fig. 4(a2). The dashed triple-peak global profile is the transmitted cavity FWM (SWM) signal induced by g^2N and E_3 when scanning Δ_1 without the dressing effect of $E_2\,(E_2')$. The three peaks correspond to the dressed states $|+\rangle$ and $|-\pm\rangle$, where the dressing effect of E_3 splits the state $|-\rangle$, dressed by g^2N, into $|-\pm\rangle$. The results by scanning Δ_2 at different Δ_1 show similar evolution with Fig. 4(a1), except that two symmetric centers ($\Delta_1/\Gamma_{20} = 226$ and $\Delta_1/\Gamma_{20} = 360$) exist in the region $\Delta_1 > 0$, caused by the interaction of the three dressing fields g^2N, E_3, and $E_2\,(E_2')$. Since the analysis method is similar to that used in Fig. 4(a1), here we give a dressed energy diagram [Fig. 4(b2)] corresponding to curve (2) to prove the left suppression and right enhancement. The enhancement conditions are $\Delta_1 + \lambda_+ + \lambda_{+\pm} = 0$

for $\Delta_1 < 0$ with $\lambda_+ = g\sqrt{N}$ and $\lambda_{+\pm} = (\Delta_2 - \lambda_+)/2 \pm \sqrt{(\Delta_2 - \lambda_+)^2/4 + |G_2|^2}$, and $\Delta_1 + \lambda_- + \lambda_{-+} + \lambda_{-+\pm} = 0$ or $\Delta_1 + \lambda_- + \lambda_{--} + \lambda_{--\pm} = 0$ for $\Delta_1 > 0$ with $\lambda_- = -g\sqrt{N}$, $\lambda_{-\pm} = -(\Delta_3 + \lambda_-)/2 \pm \sqrt{(\Delta_3 + \lambda_-)^2/4 + |G_3|^2}$, and $\lambda_{-\pm\pm} = (\Delta_2 - \lambda_{-\pm})/2 \pm \sqrt{(\Delta_2 - \lambda_{-\pm})^2/4 + |G_2|^2}$ due to the cavity transmitted signal resonating with the dressed state. The suppression condition is $\Delta_1 + \Delta_2 = 0$ for both $\Delta_1 < 0$ and $\Delta_1 > 0$ due to two-photon resonance.

Finally, we study the triply dressed transmitted cavity FWM (SWM) process when Δ_3 is scanned to discuss the suppression and enhancement effect, as shown in Fig. 4(a3). When Δ_1 is scanned without the dressing effect of E_3, the transmitted cavity FWM (SWM) spectrum with three peaks induced by g^2N and $E_2\,(E_2')$ is obtained, as the dashed curve in Fig. 4(a3). These three peaks correspond to the dressed states $|+\pm\rangle$ and $|-\rangle$, where the dressing effect of $E_2(E_2')$ splits the state $|+\rangle$, induced by g^2N, into $|+\pm\rangle$. The results by scanning Δ_3 at different Δ_1 in Fig. 4(a3) show an opposite evolution to Fig. 4(a2), because the transmitted cavity FWM (SWM) field forms a Λ-type subsystem [Fig. 4(a3)] with E_3 while a ladder-type subsystem [Fig. 4(a2)] is formed with $E_2\,(E_2')$. They have two symmetric centers ($\Delta_1/\Gamma_{20} = -357$ and $\Delta_1/\Gamma_{20} = -270$) in the region $\Delta_1 < 0$ caused by the interaction between the three dressing fields g^2N, $E_2\,(E_2')$, and E_3, and one symmetric center ($\Delta_1/\Gamma_{20} = 286$) in the region $\Delta_1 > 0$ caused by the interaction between g^2N and E_3. In this case, the enhancement condition is $\Delta_1 + \lambda_+ + \lambda_{++} + \lambda_{+++} = 0$ or $\Delta_1 + \lambda_+ + \lambda_{+-} + \lambda_{+-\pm} = 0$ for $\Delta_1 < 0$ with $\lambda_+ = g\sqrt{N}$ (induced by g^2N), $\lambda_{+\pm} = (\Delta_2 - \lambda_+)/2 \pm \sqrt{(\Delta_2 - \lambda_+)^2/4 + |G_2|^2}$ [induced by $E_2(E_2')$] and $\lambda_{+\pm\pm} = -(\Delta_3 + \lambda_{+\pm})/2 \pm \sqrt{(\Delta_3 + \lambda_{+\pm})^2/4 + |G_3|^2}$ (induced by E_3), and $\Delta_1 + \lambda_- + \lambda_{-\pm} = 0$ for $\Delta_1 > 0$ with $\lambda_- = -g\sqrt{N}$ (induced by g^2N) and $\lambda_{-\pm} = -(\Delta_3 + \lambda_-)/2 \pm \sqrt{(\Delta_3 + \lambda_-)^2/4 + |G_3|^2}$ (induced by E_3). The suppression condition is $\Delta_1 - \Delta_3 = 0$ for both $\Delta_1 < 0$ and $\Delta_1 > 0$. Here, we also give the corresponding energy level diagram to explain the curve (3) in Fig. 4(a3).

IV. VRS OF HIGH-ORDER MODES

In order to study the splitting of high-order cavity modes (multinormal mode), we adopt the intensity transmission coefficient of generated FWM (SWM) field for the coupled atoms-cavity system to discuss the splitting positions by the dressing-state theory.

The cavity transmission coefficient of FWM (SWM) field is given by [16,17]:

$$T = \frac{(t_3 t_1)^2 e^{-\alpha L_a}}{(1 - r_3 r_1 e^{-\alpha L_a/2})^2 + 4 r_3 r_1 e^{-\alpha L_a/2} \sin^2\left(\frac{\phi}{2}\right)}, \qquad (2)$$

where $\phi(\omega_{F(S)}) = 2\pi(\Delta_{ac} - \Delta_1)/\Delta_{FSR} + (n-1)L_a\omega_{F(S)}/c$ is the round-trip phase shift experienced by the intracavity field around the cavity with free spectral range (FSR) of the empty optical cavity $\Delta_{FSR} = 2\pi/(L_c/c)$ and the speed of light in vacuum c. The terms $\alpha = 2(\omega_{F(S)}/c)\mathrm{Im}[(1+\chi)^{1/2}]$ and $n = \mathrm{Re}[(1+\chi)^{1/2}]$ are the absorption coefficient and reflective index of the medium, respectively, with the susceptibility χ of the medium. In this section, we only consider the linear susceptibility, which can be derived by the master equation as

$$\chi = \frac{2g^2 N L_c}{L_a \omega_{F(S)}} \frac{i}{d_1 + |G_2|^2/d_2 + |G_3|^2/d_3}. \qquad (3)$$

The theory of the equations above can be used to discuss the splitting positions of high-order cavity modes together with the dressing-state theory in the coupled atoms-cavity system.

Figure 5 gives the transmission spectra, containing splitting positions and height of the multimode, of the generated FWM (SWM) when $\Delta_{ac} = 0$ and the power of coupling fields [$E_2\,(E_2')$ and E_3] are relatively weak (i.e., not considering their dressing effects) with the increment of the atomic density of the medium. For an empty cavity, the cavity transmission peaks are Lorentzian in shape and have equal mode spacings (Δ_{FSR}), as shown by the dashed curves in Fig. 5(a). When the coupling strength $g\sqrt{N}$ increases to near or larger than Δ_{FSR} induced by the increased atomic density of the medium in cavity, the transmission spectra can be modified significantly: Not only the zero-order longitudinal mode ($m = 0$) is split ($0_\pm$) with symmetrical center $\Delta_1 = 0$, but also high-order modes ($m = \pm1, \pm2$, etc.) are split ($1_\pm$, $-1_\pm$, $2_\pm$, $-2_\pm$, etc.) with symmetrical center $\Delta_1 = -m\Delta_{FSR}/2$ by the cavity field as the solid curves shown in Fig. 5(a). We introduce the dressing-state theory in order to understand the splitting positions of the cavity modes, still considering g^2N from the atom-cavity coupling effect as a dressing field. When a is coupled with a random cavity mode ($m = 0, \pm1, \pm2$, etc.), and after diagonalizing the interaction Hamiltonian for this atom-cavity system, the two eigenvalues corresponding to the splitting positions of peaks $m_\pm$ are derived as $\lambda_{m\pm}^{(m,\Delta_{ac})} = -(\Delta_{ac} + m\Delta_{FSR})/2 \pm \sqrt{(\Delta_{ac} + m\Delta_{FSR})^2/4 + g^2N}$ measured from cavity mode m, which means the two peaks located at $\Delta_1^{(m,\Delta_{ac})} = -m\Delta_{FSR} - \lambda_{m\pm}^{(m,\Delta_{ac})}$ relative to the position of m. Especially, when a resonates with zero-order mode ($m = 0$, $\Delta_{ac} = 0$), the splitting positions become $\Delta_1^{(0,0)} = -\lambda_{0\pm}^{(0,0)} = \mp g\sqrt{N}$ and $\Delta_1^{(1,0)} = -\Delta_{FSR} - \lambda_{1\pm}^{(1,0)} = -\Delta_{FSR}/2 \mp \sqrt{\Delta_{FSR}^2/4 + g^2N}$ corresponding to the peaks of the zero-order cavity mode and the first-order mode, which has obvious symmetrical centers $\Delta_1 = 0$ and $\Delta_1 = -\Delta_{FSR}/2$, respectively, and is in accordance with the results in Fig. 5(a). In addition, when the cavity field a resonates with other cavity modes such as $m = 1$ ($\Delta_{ac} = -\Delta_{FSR}$), the splitting positions are $\Delta_1^{(0,-\Delta_{FSR})} = -\lambda_{0\pm}^{(0,-\Delta_{FSR})} = -\Delta_{FSR}/2 \mp \sqrt{\Delta_{FSR}^2/4 + g^2N}$ and $\Delta_1^{(1,-\Delta_{FSR})} = -\Delta_{FSR} - \lambda_{1\pm}^{(1,-\Delta_{FSR})} = -\Delta_{FSR} \mp g\sqrt{N}$ corresponding to the two peaks of zero-order and first-order cavity modes. Such results demonstrate that $\Delta_1^{(1,0)} = \Delta_1^{(0,-\Delta_{FSR})}$, which means the positions of the two splitting peaks of first-order mode when a resonates with zero-order mode are the same as that of zero-order mode when a resonates with first-order mode, as shown in Fig. 5(b). Figure 5(b) presents the cavity transmitted FWM (SWM) signal as a function of Δ_1 and Δ_{ac}, with the increment of the atomic density of the medium from (b1) to (b3). They are typical avoided-crossing plots which show the splitting of the multimode due to the cavity field scanned along the horizontal axis. The smallest splitting distance is at $\Delta_{ac}/\Gamma_{20} = 0$ for zero-order mode, $\Delta_{ac}/\Gamma_{20} \approx 1000$ for negative first-order

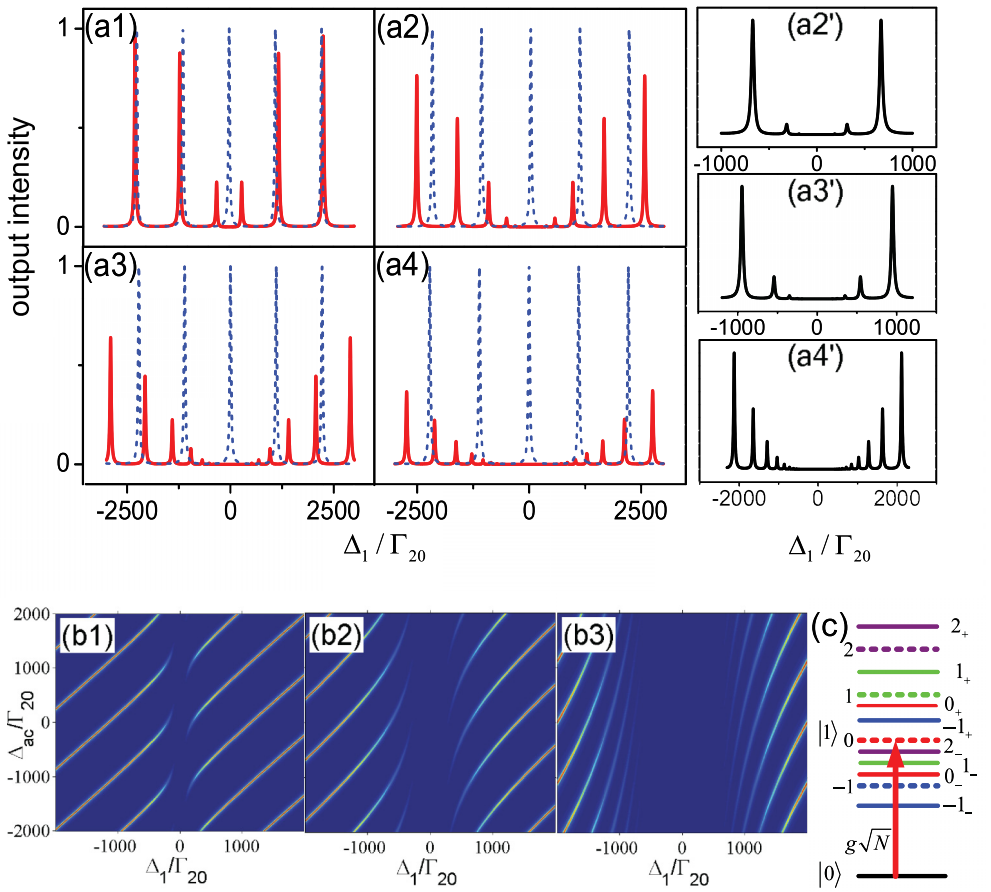

FIG. 5. (Color online) (a1)–(a4) Solid curves are transmission spectra of the generated FWM (SWM) when $\Delta_{ac} = 0$ and the powers of coupling fields [E_2 (E_2') and E_3] are relatively weak with the atomic density of the medium increasing. Dashed curves are the transmission spectra of empty cavities. The illustrations (a2′)–(a4′) show MWM transmissions in smaller regions corresponding to (a2)–(a4). (b1)–(b3) Avoided-crossing plots with increment of the atomic density of the medium. (c) The corresponding dressed energy level diagram of the system.

mode, $\Delta_{ac}/\Gamma_{20} \approx -1000$ for first-order mode, etc., and all increases with the accretion of the atomic density of the medium.

Next, we discuss the same case as Fig. 5 except that the power of E_2 (E_2') is sufficiently strong to reveal its dressing effect on cavity transmission signal with $\Delta_2 = 0$, as shown in Fig. 6. Compared with the cavity transmission spectrum in Fig. 5, the result in Fig. 6 shows an additional peak at $\Delta_1 \approx 0$ due to the frequency pulling and absorption suppression corresponding to the intracavity dark state at $\Delta_1 \approx -\Delta_2 = 0$. With the coupling strength $g\sqrt{N}$ increasing to near or larger than Δ_{FSR}, not only the zero-order mode ($m = 0$) is split into three peaks ($0_\pm$ and 0_0), but also high-order modes ($m = \pm 1, \pm 2$, etc.) are split into three peaks ($1_\pm$ and 1_0, $-1_\pm$ and -1_0, $2_\pm$ and 2_0, $-2_\pm$ and -2_0, etc.) by g^2N and E_2 (E_2'), and every pair of $m_\pm$ has a symmetrical center $\Delta_1 = -m\Delta_{FSR}/2$, shown as the solid lines in Fig. 6(a). We can apply dressing-state theory to explaining the positions of the splitting peaks as well for random cavity mode m. After diagonalizing the interaction Hamiltonian for this atom-cavity system, in which g^2N and E_2 (E_2') are considered as dressing fields and coupled with the random cavity mode ($m = 0, \pm 1, \pm 2$, etc.), we can obtain the three eigenvalues as $\lambda_{m\pm}^{(m,\Delta_{ac})} = -(\Delta_{ac} + m\Delta_{FSR})/2 \pm \sqrt{(\Delta_{ac} + m\Delta_{FSR})^2/4 + g^2N + |G_2|^2}$ and $\lambda_0^{(m,\Delta_{ac})} = -(\Delta_{ac} + m\Delta_{FSR})$ measured from cavity mode m. Thus the m-order cavity mode can be split into three peaks including two side peaks $m_\pm$ located at $\Delta_1^{(m,\Delta_{ac})} = -m\Delta_{FSR} - \lambda_{m\pm}^{(m,\Delta_{ac})}$ and a narrow peak m_0 located at $\Delta_1^{(m,\Delta_{ac})} = -m\Delta_{FSR} - \lambda_0^{(m,\Delta_{ac})}$ under superstrong-coupling condition. Similarly, we can also deduce $\Delta_1^{(1,0)} = \Delta_1^{(0,-\Delta_{FSR})}$, which means the positions of the two side peaks of the first-order mode when a resonates with zero-order mode are the same as that of the zero-order mode when a resonates with first-order mode, as can be demonstrated in Fig. 6(b). Figure 6(b) gives the cavity transmitted FWM (SWM) signal as a function of Δ_1 and Δ_{ac} with the atomic density increasing from (b1) to (b3). Similarly, they are avoided-crossing plots of the multimode, except for an additional peak at $\Delta_1 \approx 0$ due to the dressing effect of E_2 (E_2'), compared with that in Fig. 5(b).

V. STEADY-STATE LINEAR GAIN AND OPO THRESHOLD

The four-level inverted-Y system in Fig. 1(b) also may lead to three possibilities of fluorescence generation corresponding to the lambda (Λ) subsystem ($|0\rangle \rightarrow |1\rangle \rightarrow |3\rangle$ with E_1 and E_3 on) and two cascade (Ξ) subsystems ($|0\rangle \rightarrow |1\rangle \rightarrow |2\rangle$ with E_1 and E_2 on; $|3\rangle \rightarrow |1\rangle \rightarrow |2\rangle$ with E_3 and E_2 on). When

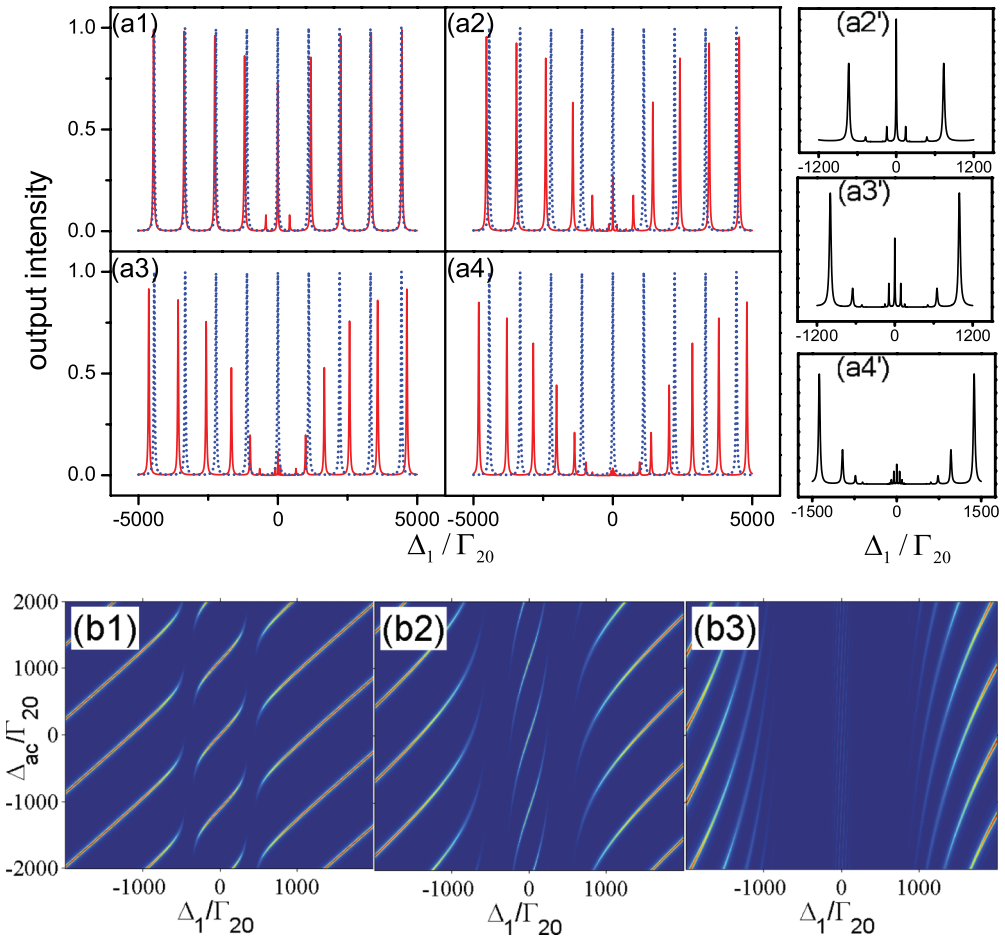

FIG. 6. (Color online) The figure setup is as Figs. 5(a) and 5(b) except that the power of E_2 (E_2') is sufficiently strong.

the fluorescence interacts with the cavity mode, the bright correlated anti-Stokes and Stokes light beams are generated [29]. We set up the theoretical model to obtain the steady-state linear gain for these generated paired beams in the above atom-cavity subsystems and get corresponding thresholds.

First we discuss the Λ-type subsystem in which E_1 resonates with transition $|0\rangle \rightarrow |1\rangle$, E_3 resonates with $|3\rangle \rightarrow |1\rangle$, and cavity field a is coupled with the two transitions so that the bright correlated light beams R_3 from $|1\rangle$ to $|3\rangle$ and R_1 from $|1\rangle$ to $|0\rangle$ can circulate in the cavity. Similar to the generation of a single bright beam [29], the two beams can couple and influence each other due to the crossed energy level for stimulation and generation. With a further consideration of the degeneracy and the collisions effect between $|3\rangle$ and $|0\rangle$ for preventing the optical pumping to $|3\rangle$, and under the steady-state approximation, we can obtain the linear gain from the coefficient of a in the expression $ig\sqrt{N}\rho_{10}$ and $ig\sqrt{N}\rho_{13}$ as

$$G_{10}^{\Lambda} = \frac{-2g^2N\left\{2G_1^2\gamma_{30}t + G_3\left(G_1+G_3\right)\left[2\Gamma_{30}\left(\gamma_{10}+\gamma_{30}-\gamma_{03}\right)-\gamma_{03}t\right]+\Gamma_{13}\Gamma_{30}\gamma_{30}t\right\}}{\left\{\left[2sG_1+\Gamma_{10}h\right]\left(G_1^2+\Gamma_{13}\Gamma_{30}\right)+\left[2qG_1^2+\Gamma_{13}h\right]\left(G_3^2+\Gamma_{10}\Gamma_{30}\right)-x+G_1^2G_3^2\left(-6\gamma_{30}+12\Gamma_{30}+2t-6\gamma_{03}\right)\right\}G_1}, \tag{4a}$$

$$G_{13}^{\Lambda} = \frac{-g^2N\left\{3G_3^2\gamma_{03}t + G_1\left(G_1+2G_3\right)\left[2\Gamma_{30}\left(\gamma_{03}+\gamma_{13}-\gamma_{30}\right)-\gamma_{30}t\right]+\Gamma_{10}\Gamma_{30}\gamma_{03}t\right\}}{\left[2sG_1+\Gamma_{10}h\right]\left(G_1^2+\Gamma_{13}\Gamma_{30}\right)+\left[2qG_1^2+\Gamma_{13}h\right]\left(G_3^2+\Gamma_{10}\Gamma_{30}\right)-x+G_1^2G_3^2\left(-6\gamma_{30}+12\Gamma_{30}+2t-6\gamma_{03}\right)}, \tag{4b}$$

where $h = \gamma_{03}\gamma_{10}+\gamma_{03}\gamma_{13}+\gamma_{10}\gamma_{30}+\gamma_{13}\gamma_{30}$, $q = \gamma_{10}+2\gamma_{03}+\gamma_{30}$, $s = \gamma_{13}+\gamma_{03}+2\gamma_{30}$, $x = \Gamma_{10}\Gamma_{13}\Gamma_{30}h$, and $t = \gamma_{10}+\gamma_{13}$. There will be linear gain for both the bright correlated light beams when $G_{10}^{\Lambda} > 0$ and $G_{13}^{\Lambda} > 0$ are simultaneously satisfied, which means that the two beams can both oscillate above these two thresholds with narrowed linewidths when we adjust G_1 and G_3. We create a possible method to control the experimental conditions to satisfy the thresholds condition from Eqs. (4), in which Γ_{30} should be very small so that it can be neglected and $\gamma_{10}+\gamma_{13}+6\Gamma_{30} > 3(\gamma_{03}+\gamma_{30})$ to guarantee positive denominators. Moreover, a crucial requirement is that $[2p^2/(1+p)] < [\gamma_3/\gamma_{30}] < [(p^2+2p)/3]$ where $p = G_1/G_3$ ($0 < p < 1$ or $p > 2$), which provides two possible ways to be experimentally achieved. When in the boundary of thresholds, we can hold G_1 as a constant while increasing G_3 with $G_3 > G_1$, or we can hold G_3 as a constant while increasing G_1 with $G_1 > 2G_3$.

A Ξ-type subsystem $|0\rangle \rightarrow |1\rangle \rightarrow |2\rangle$, in which E_1 resonates with $|0\rangle \rightarrow |1\rangle$, E_2 resonates with $|2\rangle \rightarrow |1\rangle$, and cavity field a couples with the two transitions, leads to the similar result that bright correlated light beams R_2 from $|2\rangle$ to $|1\rangle$ and R_1 from $|1\rangle$ to $|0\rangle$ can circulate and affect each other in the cavity. Meanwhile, we also assume the conditions $\rho_{00}+\rho_{11}+\rho_{22}=1$, $\rho_{10}=-\rho_{01}$, and $\rho_{21}=-\rho_{12}$. Considering an approximation of the neglected crossed influence of the cavity field, we get the steady-state linear gain as

$$G_{10}^{\Xi}=\frac{g^2N\left\{3\gamma_{21}G_1^2n+\Gamma_{21}\Gamma_{20}\gamma_{21}n+G_2^2\left[\gamma_{03}(\gamma_{10}-\gamma_{21})+2\Gamma_{20}n\right]\right\}}{\left[2(\gamma_{03}+2\gamma_{21})G_1^2+\Gamma_{10}l\right]\left(G_1^2+\Gamma_{21}\Gamma_{20}\right)+\left[2uG_2^2+\Gamma_{21}l\right]\left(G_2^2+v\right)-\Gamma_{21}vl+G_2^2G_1^2(-6\gamma_{03}+12\Gamma_{20}+2j)}, \tag{5a}$$

$$G_{21}^{\Xi}=\frac{g^2N\left\{3\gamma_{03}G_2^2j+\Gamma_{20}\Gamma_{10}\gamma_{03}j+G_1^2\left[\gamma_{21}(2\gamma_{03}-\gamma_{10})+2\Gamma_{20}(2\gamma_{03}-\gamma_{21})\right]\right\}}{\left[2(2\gamma_{03}+3\gamma_{21})G_1^2+\Gamma_{10}l\right]\left(G_1^2+v\right)+\left[2uG_2^2+\Gamma_{21}l\right]\left(G_2^2+\Gamma_{20}\Gamma_{10}\right)-\Gamma_{10}vl+G_1^2G_2^2(16\Gamma_{20}-8\gamma_{03}+2j)}, \tag{5b}$$

where $l=\gamma_{10}\gamma_{03}+\gamma_{10}\gamma_{21}+\gamma_{03}\gamma_{21}$, $u=2\gamma_{03}+\gamma_{10}$, $v=\Gamma_{21}\Gamma_{20}$, $j=\gamma_{10}-\gamma_{21}$, and $n=\gamma_{03}-\gamma_{10}$ for simplification. Similarly, to observe the two bright correlated light beams, it requires $G_{10}^{\Xi}>0$ and $G_{21}^{\Xi}>0$ and then it can be easily concluded that $\gamma_{03}>\gamma_{10}>\gamma_{21}$ is necessary with $6\Gamma_{20}+\gamma_{10}>3\gamma_{03}+\gamma_{21}$ for $G_{10}^{\Xi}>0$ while $8\Gamma_{20}+\gamma_{10}>\gamma_{21}+4\gamma_{03}$ is necessary for $G_{21}^{\Xi}>0$. It indicates that when it meets the demands of the thresholds above, two bright correlated light beams can oscillate simultaneously by increasing G_1 and G_2 or by just increasing one of them. Analogically, we can also get the gain and threshold of the other Ξ subsystem $|3\rangle \rightarrow |1\rangle \rightarrow |2\rangle$ so here we do not show more details.

It is known that the three pairs of fluorescence signals can amplify the injected vacuum field in free space. Similarly, if a MWM signal is injected and interacts with the fluorescence signals, it can be amplified as well. In our atom-cavity system (Fig. 1), if considering the bright correlated light beams [29], an OPA process will occur when we inject the FWM and SWM signals. The FWM and SWM signals can be amplified and squeezed better in the interaction with the bright correlated light beams, which can lead to a two-mode squeezing process between FWM and SWM signals, and this kind of squeeze can be used in quantum entanglement processing.

VI. OB BEHAVIOR OF MWM

In this section, in order to get a more comprehensive understanding of the intracavity influence of dark and bright states in the MWM process, we further study the OB behavior resulting from the self-Kerr nonlinear effect in the atom-cavity system as shown in Fig. 1(a). Considering relatively large self-Kerr nonlinearity susceptibility, which mainly functions as an un-neglected feedback effect (also a self-dressing effect) of the cavity in the MWM process, we investigate the OB phenomenon based on master equation formalism and the cavity transmission coefficient and conclude that there is coexistence and cascade competition of the VRS and OB behavior.

A. OB of zero-order mode

First, we analyze OB behavior of the zero-order mode based on the master equation formalism theory. Since the generated FWM (SWM) field can circulate in the ring cavity while the probe field and other coupling fields cannot, we only consider the generated FWM (SWM) field to form a cavity mode. Clearly, the generated FWM (SWM) cavity mode has a self-dressing effect of $|G_{\mathrm{F}}|^2$, which is derived from the relatively strong feedback effect. This self-dressing effect has similar influence with the self-dressing effect of g^2N, the internal-dressing effects of $|G_2|^2$, and the external-dressing effect of $|G_3|^2$, which can together result in a close interaction between VRS and OB. Here, we take the transmitted cavity FWM signal, for example, which can be obtained from Eq. (1) as

$$a_{FWM}\propto\frac{ig\sqrt{N}G_1G_2(G_2')^*}{d_4d_2(d_1)^2\left(d_1+\frac{g^2N}{d_4}+\frac{|G_2|^2}{d_2}+\frac{|G_3|^2}{d_3}+\frac{|G_{\mathrm{F}}|^2}{\Gamma_{00}}\right)}, \tag{6}$$

where the internal-dressing effect of E_2 and the external-dressing effect of E_3 are both included when the powers of E_2 and E_3 are sufficiently strong. For a perfectly tuned ring cavity, the output intensity I_o (a function in proportion, not the experimental output intensity) of the transmitted cavity FWM field is proportional to $|a_{FWM}|^2$, while the input intensity I_i of the incident field is proportional to $|G_1|^2$. So the input-output relationship can be expressed as

$$\frac{I_o}{I_i}\propto\left|ig\sqrt{N}G_2(G_2')^*\left[d_4d_2d_1^2\left(d_1+\frac{g^2N}{d_4}+\frac{|G_2|^2}{d_2}+\frac{|G_3|^2}{d_3}+\frac{I_o}{\Gamma_{00}}\right)\right]^{-1}\right|^2, \tag{7}$$

where I_o on the right-hand side describes the feedback effect of the cavity for the transmitted cavity signal. There is a cascade relationship between I_o and g^2N on the right-hand side of Eq. (7), with I_o, coming from $|G_{\mathrm{F}}|^2$, serving as the essential feedback effect in the origin of OB while g^2N serves as the essential atom-cavity coupling effect in the origin of VRS. Such relationship indicates the cascade coexistence and competition between OB and VRS.

We numerically study the input-output intensity relationship under the steady-state condition with relatively weak E_2 field and without E_3 field as shown in Fig. 7, which displays OB behavior of the transmitted cavity FWM signal influenced by I_i and Δ_1. Here the mode splitting is different from the normal VRS (only from g^2N in Sec. III) because the modes after splitting are all inclined for the feedback effect (self-dressing effect); however, the major splitting law

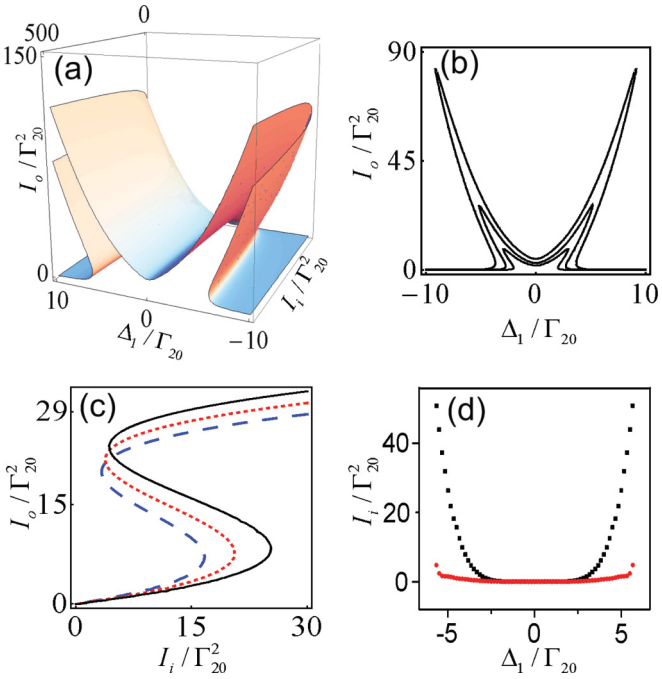

FIG. 7. (Color online) Observed input-output intensity relationship of the system with probe detuning Δ_1/Γ_{20} scanned when only zero-order cavity mode is considered, and E_2 (E_2') is relatively weak while E_3 and E_3' are blocked. (a) FWM transmission output changes with both probe detuning and probe input intensity; (b) FWM transmission output with probe detuning at different probe input intensity $I_i/\Gamma_{20}^2 = 0.1,1,10$ from inside to outside; (c) OB at different probe detunings $\Delta_1/\Gamma_{20} = 4.5$ (dashed), $\Delta_1/\Gamma_{20} = 4.7$ (dotted), and $\Delta_1/\Gamma_{20} = 4.9$ (solid); (d) probe input intensity versus Δ_1/Γ_{20} with the dots of the upper branch standing for the right OB threshold of the OPA FWM process and the dots of the lower branch standing for the left one.

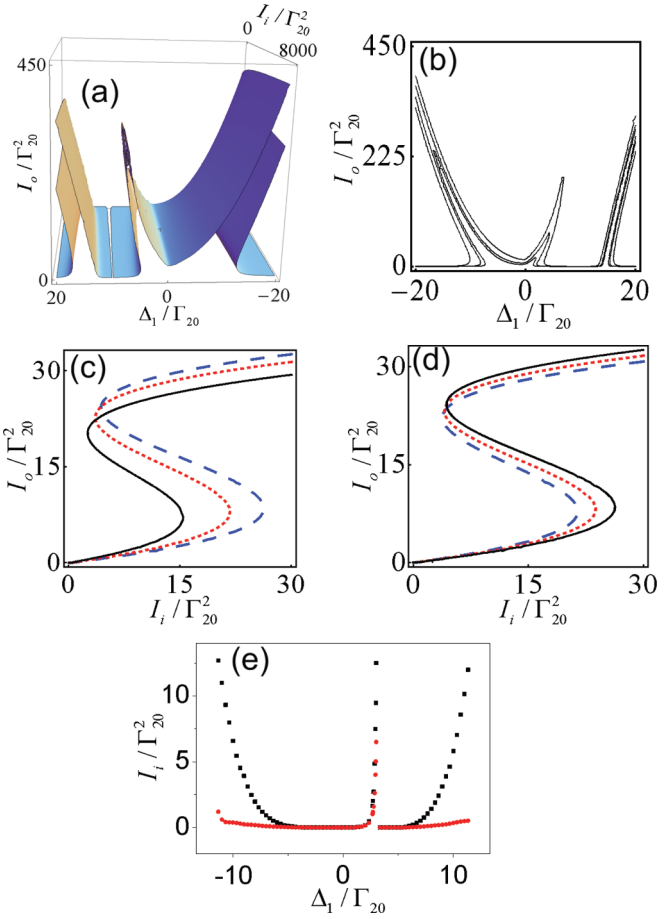

FIG. 8. (Color online) Observed input-output intensity relationship characteristics of the system with probe detuning Δ_1/Γ_{20} scanned when only the zero-order cavity mode is considered; E_2 (E_2') is sufficiently strong while E_3 and E_3' are blocked. (a) FWM transmission output changes with both probe detuning Δ_1/Γ_{20} and probe input intensity I_i/Γ_{20}^2 when G_2 is sufficiently strong; (b) FWM transmission output with probe detuning at $I_i/\Gamma_{20}^2 = 10, 50, 680$ from inside to outside; (c) FWM transmission output intensity with probe input intensity when $G_2/\Gamma_{20} = 1$ (dashed), $G_2/\Gamma_{20} = 2$ (dotted), and $G_2/\Gamma_{20} = 3$ (solid); (d) FWM transmission output intensity with probe input intensity at $\Delta_1/\Gamma_{20} = 4.8$ (dashed), $\Delta_1/\Gamma_{20} = 4.9$ (dotted), and $\Delta_1/\Gamma_{20} = 5$ (solid); (e) the OB threshold of the OPA FWM process versus Δ_1/Γ_{20} for $G_2/\Gamma_{20} = 2$ at $\Delta_2/\Gamma_{20} = -10$ with the dots of the upper branch standing for the right OB threshold and the dots of the lower branch standing for the left one.

is just the same with VRS. The inclined VRS results from the relatively large feedback effect ($|G_F|^2$) and g^2N, leading to the conclusion that there exists a strong cascade interaction between VRS and OB. Figure 7(a) illustrates the intensity of the output transmitted cavity FWM signal as the functions of I_i and Δ_1, which reveals the OB threshold of the OPA FWM process and hysteresis cycle obviously with the variation of Δ_1. These modulations of the VRS in frequency domain and input-output relationship (OB behavior) simultaneously result from the significant change of the absorption and dispersion characteristics of the medium. In detail, Fig. 7(b) shows the transmitted cavity FWM signal expanding rapidly with I_i increasing when Δ_1 is scanned. Increased $|\Delta_1|$ results in a significant change of the OB behavior and the increasing of the right OB threshold as in Fig. 7(c). Figure 7(d) displays the OB threshold values versus Δ_1, in which the left OB threshold value shifts slowly while the right one shifts sharply. Moreover, Fig. 7(d) also demonstrates that the OB always exists in a certain sideband region corresponding to the generated inclined peaks after splitting, and there is no OB at or close to the point $\Delta_1/\Gamma_{20} = 0$ (dark state) whatever the probe input intensity is, which results from disappearance of the linear dispersion at the line center ($\Delta_1/\Gamma_{20} = 0$) by the interference between two possible absorption channels $|0\rangle \rightarrow |\pm\rangle$ induced by g^2N. This interesting result enables us to make the following study to verify the primary conclusion that OB does not exist at or near all the positions of dark states induced by the dressing fields.

Analogically, we analyze the similar dependence of OB behavior when the power of E_2 is sufficiently strong to reveal its dressing effect, as shown in Fig. 8. The basic OB characteristic is in accordance with the previous analysis. As a consequence of the dressing effect of E_2, the absorption and dispersion coefficient of the medium can be modified dramatically, which results in the AT splitting based on the VRS and the three different frequency (Δ_1) regions of the

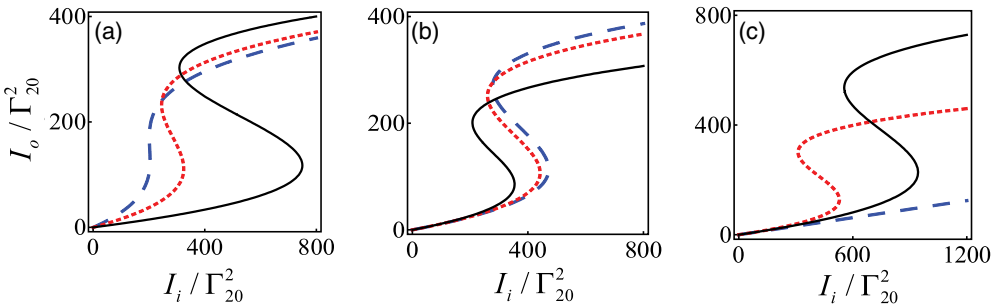

FIG. 9. (Color online) FWM transmission output intensity versus probe input intensity when E_2 (E_2') is sufficiently strong with E_3 and E_3' blocked. The dashed, dotted, and solid curves correspond to (a) N decreases as $N/\Gamma_{20} = 100, 10, 1$; (b) the Rabi frequency of dressing field increases as $G_2/\Gamma_{20} = 0, 2, 4$; (c) different detuning combinations $\Delta_1 + \Delta_2 = 0, 0.5, -0.5$ are adopted when $G_2/\Gamma_{20} = 2$.

OB, shown as Figs. 8(a) and 8(b). Figure 8(c) illustrates the fierce decreasing of the two OB threshold values of the OPA FWM process when increasing the Rabi frequency of E_2 as $G_2/\Gamma_{20} = 1, 2, 3$, especially the right one. Figure 8(d) displays the decreasing OB threshold values with decreasing $|\Delta_1|$, the same as in Fig. 7(c). Also, there is no OB at the position of the dark state ($\Delta_1/\Gamma_{20} = 0$ and $\Delta_1 + \Delta_2 = 0$), due to the lack of linear dispersion induced by $g^2 N$ and the suppression effect induced by E_2, as predicted by Fig. 8(e). The phenomena in this part demonstrate the changeable properties of OB behavior influenced by the dark state induced by the dressing effect, and we believe this will provide a kind of experimental control of VRS and OB simultaneously.

B. OB of high-order modes

On the other hand, we consider the OB of high-order modes theoretically based on the traditional cavity transmission coefficient as contrast and also take the transmitted FWM signal, for example. The total susceptibility can be expressed as $\chi = \chi^{(1)} + \chi^{(3)} |E_i|^2 = N\mu_{10}^2(\tilde{\rho}_{10}^{(1)} + \tilde{\rho}_{10}^{(3)})/[\varepsilon_0 \hbar G_F]$, in which $\chi^{(1)}$ and $\chi^{(3)}$ are the linear susceptibility and the third-order nonlinear susceptibility, respectively. Here, we can obtain $\tilde{\rho}_{10}^{(1)}$ and $\tilde{\rho}_{10}^{(3)}$ by solving the coupled density-matrix equations as

$$\tilde{\rho}_{10}^{(1)} = \frac{i G_F}{d_1 + \frac{|G_2|^2}{d_2} + \frac{|G_3|^2}{d_3}}, \tag{8}$$

$$\tilde{\rho}_{10}^{(3)} = \frac{-i G_F |G_F|^2}{\left[d_1 + \frac{|G_2|^2}{d_2} + \frac{|G_3|^2}{d_3}\right]^3} + \frac{-i G_F |G_1|^2}{\left[d_1 + \frac{|G_2|^2}{d_2} + \frac{|G_3|^2}{d_3}\right]^3} + \frac{-i G_F |G_2|^2}{\left[d_1 + \frac{|G_2|^2}{d_2} + \frac{|G_3|^2}{d_3}\right]^2 d_2} + \frac{-i G_F |G_3|^2}{\left[d_1 + \frac{|G_2|^2}{d_2} + \frac{|G_3|^2}{d_3}\right]^2 d_3}. \tag{9}$$

In Eq. (9), the first term in $\tilde{\rho}_{10}^{(3)}$ indicates the self-Kerr effect while the last three terms indicate the cross-Kerr effect in medium. Consider that $|G_F|^2$ is proportional to the intensity of the transmitted cavity FWM field when the feedback effect is considered. So the susceptibility can be revised as

$$\chi = \frac{2g^2 N L_c}{L_a \omega_1} \left\{ \frac{i}{d_1 + \frac{|G_2|^2}{d_2} + \frac{|G_3|^2}{d_3}} + \frac{-i I_o}{\left[d_1 + \frac{|G_2|^2}{d_2} + \frac{|G_3|^2}{d_3}\right]^3} + \frac{-i |G_1|^2}{\left[d_1 + \frac{|G_2|^2}{d_2} + \frac{|G_3|^2}{d_3}\right]^3} + \frac{-i |G_2|^2}{\left[d_1 + \frac{|G_2|^2}{d_2} + \frac{|G_3|^2}{d_3}\right]^2 d_2} + \frac{-i |G_3|^2}{\left[d_1 + \frac{|G_2|^2}{d_2} + \frac{|G_3|^2}{d_3}\right]^2 d_3} \right\}. \tag{10}$$

Then based on Eq. (2), the OB can be investigated.

By setting the relevant parameters at appropriate values, we can increase $g\sqrt{N}$ to be near or larger than Δ_{FSR} so as to observe the OB of high-order modes, and the OB still only appears at the position where absorption and dispersion are appropriate under the influence of splitting. Now we succeed in controlling their OB thresholds of the OPA FWM process and curve shape by adjusting several related parameters. When there is one dressing field and only the self-Kerr nonlinearity effect is considered, the corresponding results are shown in Fig. 9. When N decreases as in Fig. 9(a), the left OB threshold increases slowly while the right one increases sharply, leading to a dramatic expansion of the bistable region. Similarly, if we increase the intensity of the dressing field as in Fig. 9(b), both the two OB thresholds decrease and the size of the bistable region just nearly stays the same. Finally, we discuss the OB at $\Delta_1 + \Delta_2 = 0, 0.5, -0.5$ as shown in Fig. 9(c). As what we have assumed according to the analysis previously, there is no OB effect at the dark-state position and the OB will gradually appear when the frequency detuning deviates from $\Delta_1 + \Delta_2 = 0$ step by step. All the results reveal that the origin of the OB is related with the splitting of the cavity modes to some extent, and we can apply this kind of control of the OB threshold of the OPA FWM process to the development of an OB switch.

VII. CONCLUSION

In conclusion, we have investigated the control of the dark state on the multidressed VRS and OB behavior of a zero- and high-order transmitted cavity MWM signal in the

coupled system consisting of a specific ring cavity and reverse Y-type four-level atoms assembly. The numerical calculations are based on the master equation formalism and the traditional cavity transmission coefficient. We have demonstrated the coexistence and cascade competition between VRS and OB behavior, where the VRS results from the atom-cavity collective effect induced by high atom density while the OB behavior results from the sufficiently strong feedback effect. Due to the complicated generation and operation process of the MWM signal, the inclined VRS is obtained under the interaction with OB, and such OB behavior cannot appear at or near the position of the dark state induced by the dressing effect. We also demonstrate the suppression and enhancement of the multidressed MWM signal by scanning the frequency detuning of the dressing field, and the linear gains and thresholds for the paired bright correlated light beams in the OPO process with an OB threshold of the OPA MWM process. Such control of dark and bright states on the VRS and OB, etc., can be achieved by adjusting the cavity field and other coupling fields, and will be useful in potential applications for optical devices and quantum information projects.

ACKNOWLEDGMENTS

This work was supported by the 973 Program (Grant No. 2012CB921804), NSFC (Grants No. 10974151, No. 61078002, No. 61078020, No. 11104214, No. 61108017, No. 11104216, and No. 61205112), NCET (Grant No. 08-0431), RFDP (Grants No. 20110201110006, No. 20110201120005, and No. 20100201120031), FRFCU (Grants No. 2012jdhz05, No. 2011jdhz07, No. xjj2011083, No. xjj2011084, No. xjj20100151, No. xjj20100100, and No. xjj2012080), and CPSF (Grant No. 2012M521773).

APPENDIX A: CALCULATION OF TRANSMITTED CAVITY MODE

In this Appendix, we give more detail of the calculation of transmitted cavity mode induced by FWM (SWM) and doubly dressed by E_2 (or E_2') and E_3, shown as Eq. (1) in the text.

Under the weak-cavity field limitation and with all the atoms initially in the ground state $|0\rangle$, the evolution of the cavity field and the density matrix operators obey the following linear equations, which can be easily derived using the master equation in the atom-cavity interaction picture:

$$\dot{a} = -[i(\Delta_1 - \Delta_{ac}) + \gamma]a + ig\sqrt{N}\rho_{10}, \tag{A1}$$

$$\dot{\rho}_{10} = -[i\Delta_1 + \Gamma_{10}]\rho_{10} + iG_{F(S)}\rho_{00} + ig\sqrt{N}a\rho_{00} + iG_2^*\rho_{20} + iG_3\rho_{30}, \tag{A2}$$

$$\dot{\rho}_{20} = -[i(\Delta_1 + \Delta_2) + \Gamma_{20}]\rho_{20} + iG_2\rho_{10}, \tag{A3}$$

$$\dot{\rho}_{30} = -[i(\Delta_1 - \Delta_3) + \Gamma_{30}]\rho_{30} + iG_3^*\rho_{10}. \tag{A4}$$

Here the overdots represent the derivative with respect to time t, γ is the decay rate for the cavity, ρ_{ij} is the density matrix element, $\Delta_{ac} = \omega_{10} - \omega_c$ is the detuning of the cavity field with cavity frequency ω_c, and $G_{F(S)}$ is the Rabi frequency of the generated FWM (SWM) field with $G_F \propto \sqrt{2/\varepsilon_0 c\hbar}N\mu^2\rho_{F2}^{(3)}$, $G_S \propto \sqrt{2/\varepsilon_0 c\hbar}N\mu^2\rho_{S3}^{(5)}$. Due to the results of the above equations and equilibrium state of the system, we can acquire the transmitted cavity mode induced by FWM (SWM) and doubly dressed by E_2 (or E_2') and E_3.

APPENDIX B: CALCULATION OF STEADY-STATE LINEAR GAIN

The steady-state linear gains that are only alluded to in the text are given more detailed calculations in this Appendix.

In the Λ-type subsystem mentioned in the text in which E_1 resonates with transition $|0\rangle \to |1\rangle$, E_3 resonates with $|3\rangle \to |1\rangle$, and cavity field a is coupled with the two transitions, the evolution of density matrix elements are

$$\dot{\rho}_{10} = -\Gamma_{10}\rho_{10} + i(G_1 + g\sqrt{N}a)(1 - \rho_{33} - 2\rho_{11}) + i(G_3 + g\sqrt{N}a)\rho_{30}, \tag{B1a}$$

$$\dot{\rho}_{30} = -\Gamma_{30}\rho_{30} + i(G_3 + g\sqrt{N}a)\rho_{10} - i(G_1 + g\sqrt{N}a)\rho_{31}, \tag{B1b}$$

$$\dot{\rho}_{13} = -\Gamma_{13}\rho_{13} + i(G_3 + g\sqrt{N}a)(\rho_{33} - \rho_{11}) + i(G_1 + g\sqrt{N}a)\rho_{30}, \tag{B1c}$$

$$\dot{\rho}_{11} = -(\gamma_{10} + \gamma_{13})\rho_{11} - 2i(G_1 + g\sqrt{N}a)\rho_{10} - 2i(G_3 + g\sqrt{N}a)\rho_{13}, \tag{B1d}$$

$$\dot{\rho}_{33} = -\gamma_{30}\rho_{33} + \gamma_{03}(1 - \rho_{11} - \rho_{33}) + \gamma_{13}\rho_{11} + 2i(G_3 + g\sqrt{N}a)\rho_{13}, \tag{B1e}$$

where γ_{ij} represents the spontaneous decay rate from $|i\rangle$ to $|j\rangle$ (γ_{10} and γ_{13}), or the decay rate from $|i\rangle$ to $|j\rangle$ (γ_{30} and γ_{03}) caused by the collision. In Eq. (B1), we assume $\rho_{00} + \rho_{11} + \rho_{33} = 1$, $\rho_{10} = -\rho_{01}$, $\rho_{13} = -\rho_{31}$, and $\rho_{30} = \rho_{03}$, which are all caused by the resonance condition. From the calculation above we can easily obtain the linear gain shown as Eqs. (4) in the text.

Similarly, in the Ξ-type subsystem $|0\rangle \to |1\rangle \to |2\rangle$ mentioned in the text in which E_1 resonates with $|0\rangle \to |1\rangle$, E_2 resonates with $|2\rangle \to |1\rangle$, and cavity field a couples with the two transitions, the evolution of the density matrix elements can be given as

$$\dot{\rho}_{10} = -\Gamma_{10}\rho_{10} + i(G_1 + g\sqrt{N}a)(\rho_{00} - \rho_{11}) + i(G_2 + g\sqrt{N}a)\rho_{20}, \tag{B2a}$$

$$\dot{\rho}_{20} = -\Gamma_{20}\rho_{20} + i(G_2 + g\sqrt{N}a)\rho_{10} - i(G_1 + g\sqrt{N}a)\rho_{21}, \tag{B2b}$$

$$\dot{\rho}_{21} = -\Gamma_{21}\rho_{21} + i(G_2 + g\sqrt{N}a)(2\rho_{11} + \rho_{00} - 1) - i(G_1 + g\sqrt{N}a)\rho_{20}, \tag{B2c}$$

$$\dot{\rho}_{11} = -\gamma_{10}\rho_{11} + \gamma_{21}(1 - \rho_{00} - \rho_{11}) - 2i(G_1 + g\sqrt{N}a)\rho_{10} + 2i(G_2 + g\sqrt{N}a)\rho_{21}, \tag{B2d}$$

$$\dot{\rho}_{00} = -\gamma_{03}\rho_{00} + \gamma_{10}\rho_{11} + 2i(G_1 + g\sqrt{N}a)\rho_{10}. \tag{B2e}$$

Then with an approximation of the neglected crossed influence of the cavity field, we get the steady-state linear gain shown as Eqs. (5) in the text.

[1] S. E. Harris, Phys. Today **50**, 36 (1997).
[2] M. Fleischhauer, A. Imamoglu, and J. P. Marangos, Rev. Mod. Phys. **77**, 633 (2005).
[3] J. G. Banacloche, Y. Li, S. Jin, and M. Xiao, Phys. Rev. A **51**, 576 (1995).
[4] L. V. Hau, S. E. Harris, Z. Dutton, and C. H. Behroozi, Nature (London) **397**, 594 (1999).
[5] M. D. Eisaman, A. Andre, F. Massou, M. Fleischhauer, A. S. Zibrov, and M. D. Lukin, Nature (London) **438**, 837 (2005).
[6] C. Liu, Z. Dutton, C. H. Behroozi, and L. V. Hau, Nature (London) **409**, 490 (2001).
[7] L. M. Duan, M. D. Lukin, J. I. Cirac, and P. Zoller, Nature (London) **414**, 413 (2001).
[8] M. D. Lukin, A. B. Matsko, M. Fleischhauer, and M. O. Scully, Phys. Rev. Lett. **82**, 1847 (1999).
[9] M. Fleischhauer and M. D. Lukin, Phys. Rev. Lett. **84**, 5094 (2000).
[10] Y. Zhu, D. J. Gauthier, S. E. Morin, Q. Wu, H. J. Carmichael, and T. W. Mossberg, Phys. Rev. Lett. **64**, 2499 (1990).
[11] R. J. Thompson, G. Rempe, and H. J. Kimble, Phys. Rev. Lett. **68**, 1132 (1992).
[12] G. S. Agarwal, Phys. Rev. Lett. **53**, 1732 (1984).
[13] M. Tavis and F. W. Cummings, Phys. Rev. **170**, 379 (1968).
[14] H. Wu, J. Gea-Banacloche, and M. Xiao, Phys. Rev. Lett. **100**, 173602 (2008).
[15] H. Wu, J. Gea-Banacloche, and M. Xiao, Phys. Rev. A **80**, 033806 (2009).
[16] X. Yu, D. Xiong, H. Chen, P. Wang, M. Xiao, and J. Zhang, Phys. Rev. A **79**, 061803 (2009).
[17] X. Yu and J. Zhang, Opt. Express **18**, 4057 (2010).
[18] S. Reynaud, C. Fabre, and E. Giacobino, J. Opt. Soc. Am. B **4**, 1520 (1987).
[19] A. S. Lane, M. D. Reid, and D. F. Walls, Phys. Rev. Lett. **60**, 1940 (1988).
[20] V. Boyer, A. M. Marino, and P. D. Lett, Phys. Rev. Lett. **100**, 143601 (2008).
[21] H. Wang, D. J. Goorskey, W. H. Burkett, and M. Xiao, Opt. Lett. **25**, 1732 (2000).
[22] A. Joshi and M. Xiao, Phys. Rev. Lett. **91**, 143904 (2003).
[23] Y. Zhang, A. W. Brown, and M. Xiao, Phys. Rev. Lett. **99**, 123603 (2007).
[24] Y. Zhang, U. Khadka, and M. Xiao, Phys. Rev. Lett. **102**, 013601 (2009).
[25] Y. Zhang, Z. Nie, Z. Wang, C. Li, F. Wen, and M. Xiao, Opt. Lett. **35**, 3420 (2010).
[26] Y. Zhang, Z. Nie, Y. Zhao, C. Li, R. Wang, J. Si, and M. Xiao, Opt. Express **18**, 10963 (2010).
[27] C. Li, Y. Zhang, Z. Nie, H. Zheng, C. Zuo, Y. Du, J. Song, K. Lu, and C. Gan, Opt. Commun. **283**, 2918 (2010).
[28] C. Li, H. Zheng, Y. Zhang, Z. Nie, J. Song, and M. Xiao, Appl. Phys. Lett. **95**, 041103 (2009).
[29] H. Wu, M. Xiao, and J. Gea-Banacloche, Phys. Rev. A **78**, 041802 (2008).